Scripta Materialia 158 (2019) 11–15

Contents lists available at ScienceDirect

Scripta Materialia

journal homepage: www.elsevier.com/locate/scriptamat

Regular article

First-order grain boundary transformations in Au-doped Si: Hybrid Monte Carlo and molecular dynamics simulations verified by first-principles calculations

Chongze Hu, Jian Luo *

Program of Materials Science and Engineering, Department of Nanoengineering, University of California, San Diego, La Jolla, CA 92093, USA

ARTICLE INFO

Article history:
Received 1 July 2018
Received in revised form 12 August 2018
Accepted 13 August 2018
Available online xxxx

Keywords:
First-order interfacial transformation
Grain boundary phase diagram
Semi-grand canonical ensemble
Hybrid Monte Carlo and molecular dynamics simulation
First-principles calculation

ABSTRACT

Hybrid Monte Carlo and molecular dynamics simulations (hybrid MC/MD) reveal the occurrence of first-order phase-like adsorption transformations in Au-doped Si twist grain boundary (GB) at low temperatures, which become continuous at high temperatures above a GB critical point. The predicted first-order GB transformations from nominally "clean" GBs to bilayer adsorption of Au are supported by a prior experiment. The hexagonal Au adsorption pattern predicted by the hybrid MC/MD simulation is further verified by first-principles calculations. Differential charge density maps indicate that strong charge transfer at the Au-doped Si GB. A GB complexion (interfacial phase) diagram is computed.

The properties of polycrystalline materials can be significantly altered by adsorption (a.k.a. segregation) of alloying elements or impurities at grain boundaries (GBs) [1–4]. Moreover, GBs can exhibit phase-like transformations [5–9]. A term "complexion" was introduced to describe the interfacial phases that are thermodynamically 2-D (despite having an effective thickness and through-thickness compositional and structural gradients), to differentiate them from thin layers of thermodynamically 3-D (bulk) Gibbs phases present at interfaces. Notably, Dillon et al. catalogued a series of six common GB complexions in doped Al_2O_3 [5,7].

Similar to bulk phase diagrams, we can construct GB diagrams to represent the stability of 2-D interfacial phases (complexions) as a function of bulk composition and temperature [6,7,10]. Specifically, bulk CALPHAD (calculation of phase diagrams) methods have been extended to GBs to construct GB λ diagrams [11–14], which have been successfully used to predict high-temperature GB disordering and related GB-controlled sintering behaviors [11,12,14–17]. Furthermore, diffuse-interface [10,18,19] and lattice-type models [20–23] have been used to compute more rigorous GB phase (complexion) diagrams with first-order transformation lines and critical points.

To further reveal atomic-level structural details underlying interfacial transformations, molecular dynamics (MD) simulations and first-principles density functional theory (DFT) calculations have been adopted. Frolov et al. applied MD and semi-grand canonical Monte Carlo (MC) simulations to investigate GB structural transformations in pure and Ag-doped Cu [24–26]. Pan et al. carried out hybrid MC/MD simulations to study segregation-induced structural transformation in Zr-doped Cu [27]. Johansson et al. also used a DFT based cluster-expansion method to construct interfacial phase diagram for V-doped WC-Co hetero-phase interface [28].

In one most recent study, Yang et al. combined a genetic algorithm with hybrid MC/MD simulations in semi-grand canonical ensembles to construct a GB "phase" (complexion) diagram for the Σ5 (210) tilt GB in Ni-doped Mo [29], which includes a first-order transition line ending at a GB critical point. Moreover, the semi-grand-canonical-ensemble simulations revealed that such first-order GB transformations break the mirror symmetry of the symmetric tilt GB [29], representing a new interfacial phenomenon discovered by atomistic simulations.

Most previous studies investigated more special GBs with relatively small Σ values, whereas more general GBs are prevailing in real polycrystalline materials and they can often be the weak link mechanically and chemically, thereby limiting the materials performance. In a prior experimental study [30], Ma et al. revealed that the Σ43 (111) twist GB in Au-doped Si exhibited an abrupt transition from "clean" GBs to bilayer adsorption of Au. However, the atomic-level details of this Au-based bilayer and its stability as a function of temperature and bulk composition have not been revealed. Motivated by this experimental observation [30], herein we combined hybrid MC/MD simulations with first-principles density functional theory (DFT) calculations to

* Corresponding author.
E-mail address: jluo@alum.mit.edu (J. Luo).

https://doi.org/10.1016/j.scriptamat.2018.08.017
1359-6462/

characterize Au-doped Si Σ43 and Σ21 (111) twist GBs, and subsequently constructed a GB adsorption diagram with a first-order transformation line and a GB critical point.

The initial undoped Σ43 GB containing 41,264 atoms with a twist angle of ~15° perpendicular to the (111) plane (matching that adopted in the prior experiment [30]) was constructed by using GBstudio [31]. An angular-dependent potential (ADP) recently developed from ab initio calculations by Starikov et al. [32] was adopted for simulating the Si—Au binary system. To test this ADP, we first calculated the Si melting temperature (T_m) and the Si—Au bulk phase diagram (Suppl. Data Fig. S1). The calculated T_m of the pure Si is around 1325 K, which is consistent with the value obtained by Starikov et al. (~1390 K) [32], but smaller than experimental value of 1689 K [33]. Yet, Starikov et al. showed that this potential is precise enough to predict the interatomic behaviors of the Si—Au binary system [32]. Consistently, the liquidus line in our calculated phase diagram (Suppl. Data Fig. S1) match well with experiment, but the solid solubilities of Au in Si obtained are higher. For a better composition with the experiment, we normalize temperature to the calculated T_m of Si and bulk composition (X_{Au}) to the maximum solid solubility from the simulation ($X_{Max\ Solubility}$) to represent our computed results.

Before simulating Au-doped Si GBs, undoped Si GBs were first annealing at ~0.75 T_m for 1 ns with a time step 1 fs via MD simulation under constant NPT. Subsequently, hybrid MC/MD simulations were carried out to introduce Au atoms at a fixed chemical potential difference of $\Delta\mu \equiv \Delta\mu_{Si} - \Delta\mu_{Au}$, in semi-grand canonical ensembles. In each MC/MD step, five MC trial moves were performed (for up to five atoms) between each MD step (for all atoms in the cell) with 1 fs MD time step; 1 million hybrid MC/MD steps were typically performed for each simulation. Further details of this hybrid MC/MD simulation procedure can also be found in a prior study of a different system [29].

Fig. 1(a) shows a simulated atomic structure of the undoped Si Σ43 GB relaxed by MD at 0.75 T_m. An associated simulated STEM high-angle annual dark-field (HAADF) micrograph is displayed in Fig. 1(b), which agrees well with experimental STEM HAADF image shown in Fig. 1(c) from Ref. [30]. The atomic structure of the Au-doped Si Σ43 GB obtained via hybrid MC/MD simulation (at $T = 0.60\ T_m$ and $\Delta\mu = -0.3$ eV) is displayed in Fig. 1(d). The Au atomic distribution along z direction (c.f. inset in Fig. 1(d)) shows that most Au atoms (represented by red dots in Fig. 1(d)) segregate/adsorb at the GB with a bilayer-like distribution, which matches the two bright fringes in the simulated (Fig. 1(e)) and experimental (Fig. 1(f)) STEM HAADF images. All STEM simulations were performed by QSTEM program under the STEM mode [34,35]; the orientations of atomistic configurations were selected to match with experimental STEM micrographs. We have also simulated STEM images on quenched atomistic structures (by MD at 10 K for 10 ps) to make sure that thermal noises do not alter the final STEM images appreciably. The different contrasts in simulated and experimental HAADF images may be due to the different specimen thickness and STEM conditions; nonetheless, both of them exhibit two bright fringes as signatures of the Au-based bilayers.

To investigate possible adsorption transitions, we calculated GB excess of Au (i.e., the amount of adsorption, Γ_{Au}) as a function of normalized temperature and composition. Fig. 2(a) shows a GB adsorption diagram at the high-temperature range from 0.53–0.83 T_m. Fig. 2(b) further shows a close-up of the computed GB adsorption diagram at the low-temperature, low-Au-content region, where a first-order GB transformation line has been identified. This first-order phase-like transformation line ends at a GB critical point at ~0.38 T_m; see discussion below and further details on identifying this GB critical point in Suppl. Data Fig. S2. Fig. 2(b) represents a computed GB complexion (2D interfacial phase) diagram.

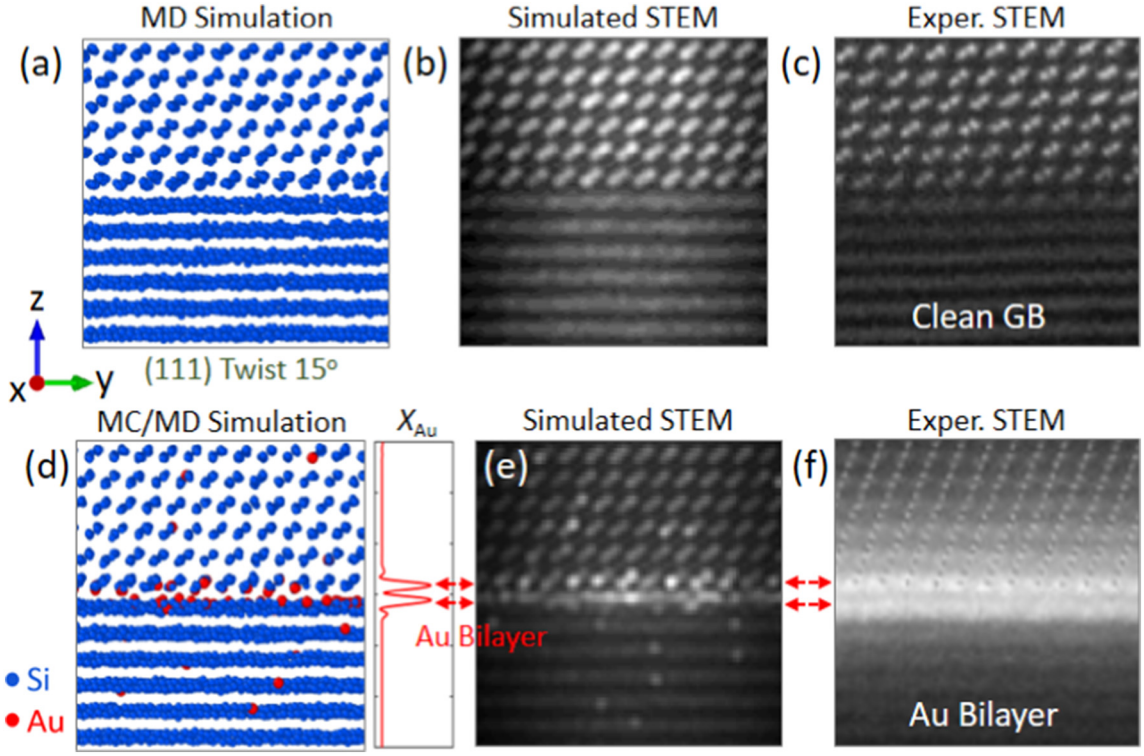

Fig. 1. (a) The atomic structure of the undoped Si Σ43 (111) twist GB obtained by MD simulations at $T = 0.75\ T_m$ and (b) the associated simulated STEM HAADF micrograph, along with (c) an experimental STEM HAADF micrograph from Ref. [30]. (d) The atomic structure of the Au-doped Si Σ43 GB obtained by hybrid MC/MD simulation at $T = 0.60\ T_m$ and $\Delta\mu = -0.3$ eV. The inset is the Au atomic fraction (X_{Au}) averaged along the z direction. (e) A simulated STEM HAADF micrograph from the hybrid MC/MD simulated interfacial structure, and (f) an experimental STEM HAADF micrograph from Ref. [30]. The brightness and contrast of the experimental micrographs are adjusted to roughly match those of simulated images. (For interpretation of the references to color in this figure, the reader is referred to the web version of this article.)